Robotica (2019) volume 37, pp. 837–850. © Cambridge University Press 2019
doi:10.1017/S0263574718001352

A Simple Two-step Geometric Approach for the Kinematic Calibration of the 3-PRS Parallel Manipulator

Genliang Chen†*, Lingyu Kong‡, Qinchuan Li¶ and Hao Wang†

† *State Key Laboratory of Mechanical Systems and Vibration, Shanghai Key Laboratory of Digital Manufacturing for Thin-Wall Structures, Shanghai Jiao Tong University, Shanghai 200240, China*
‡ *Intelligent Robot Research Center, Zhejiang Lab, Hangzhou 311100, China*
¶ *The Mechatronic Institute, Zhejiang Sci-Tech University, Hangzhou 310018, China*

(Accepted November 30, 2018. First published online: January 14, 2019)

SUMMARY
Kinematic calibration plays an important role in the improvement of positioning accuracy for parallel manipulators. Based on the specific geometric constraints of limbs, this paper presents a new kinematic parameter identification method for the widely studied 3-PRS parallel manipulator. In the proposed calibration method, the planes where the PRS limbs exactly located are identified firstly as the geometric characteristics of the studied parallel manipulator. Then, the limbs can be considered as planar PR mechanisms whose kinematic parameters can be determined conveniently according to the limb planes identified in the first step. The main merit of the proposed calibration method is that the system error model which relates the manipulator's kinematic errors to the output ones is not required for kinematic parameter identification. Instead, only two simple geometric problems need to be established for identification, which can be solved readily using gradient-based searching algorithms. Hence, another advantage of the proposed method is that parameter identification of the manipulator's limbs can be accomplished individually without interactive impact on each other. In order to validate the effectiveness and efficiency of the proposed method, calibration experiments are conducted on an apparatus of the studied 3-PRS parallel manipulator. The results show that using the proposed two-step calibration method, the kinematic parameters can be identified quickly by means of gradient searching algorithm (converge within five iterations for both steps). The positioning accuracy of the studied 3-PRS parallel manipulator has been significantly improved by compensation according to the identified parameters. The mean position and orientation errors at the validation configurations have been reduced to 1.56×10^{-4} m and 1.13×10^{-3} rad, respectively. Further, the proposed two-step kinematic calibration method can be extended to other limited-degree-of-freedom parallel manipulators, if proper geometric constraints can be characterized for their kinematic limbs.

KEYWORDS: Kinematic calibration; Parallel manipulator; Error modeling; Geometric approach.

1. Introduction

Limited degree-of-freedom (DOF) parallel mechanisms have a wide range of industrial applications, such as the high-speed pick-and-place devices,[1] heavy-duty manipulators,[2–4] and high-precision machine tools.[5–7] In these applications, the positioning accuracy of the manipulator's end-effector becomes one of the most important performance indices.[8] Due to the existences of manufacturing and assembling tolerances, there inevitably exist deviations between the kinematic parameters' actual values and their nominal ones, which significantly reduces the absolute positioning accuracy of

* Corresponding author. E-mail: leungchan@sjtu.edu.cn

the manipulators. As a result, kinematic calibration is usually conducted as an economical and effective way to overcome this problem by correcting the inaccurate kinematic parameters in the control algorithm.[9–13] For conventional serial robots, the issue of kinematic calibration has been intensively studied and many systematic approaches[14–16] have been proposed during the past decades. However, for parallel manipulators, especially those limited-DOF ones, this problem is still far from being complete, although a lot of related research has been reported in the literature recently.

As it is known, kinematic calibration of robot manipulators includes four aspects: error modeling, configuration measurement, parameter identification, and compensation control. Among these, error models play an important role, which provide an explicit relation between the parameter inaccuracy and the output errors. Due to the complexity of forward kinematics, inverse kinematics is usually utilized to establish the error models of parallel manipulators.

Masory et al.[17,18] presented a systematic investigation on the kinematic calibration of the well-known Stewart platform based on its inverse kinematics. Hollerbach and Lokhorst[19] developed a closed-loop calibration method for the kinematic parameter identification of the RSI 6-DOF parallel mechanism. Based upon this, the error models of 6-PUS and 6-PSS parallel manipulators were established by disturbance method, and the cost functions were defined as the residuals of the link lengths.[20,21] Zhuang et al.[22,23] proposed the concept of self-calibration for kinematic calibration of Stewart platforms by minimizing the residuals of inverse kinematics. To overcome shortages and embrace merits of existing approaches, Chiu and Perng[24] also presented a self-calibration strategy of a general hexapod parallel manipulator by means of using redundant sensors. By imposing specific external position constraints, Rauf and Ryu[25] established an autonomous calibration technique to identify the kinematic parameters of the 6-DOF Hexa-slide parallel manipulator. Huang et al.[26] also proposed an external calibration approach that enables the geometric parameter errors of 6-DOF parallel kinematic machines using a minimum set of pose error measurements. Taking the 6-DOF Hexapod parallel manipulator as an example, Chen et al.[27] proposed an optimal kinematic calibration method using a new observability index based on the infinity-norm assessment of the residual errors. Generally, for the 6-DOF parallel manipulators, the error models can usually be established readily by minimizing the residual link lengths of all limbs. However, for limited-DOF parallel manipulators, the problem of error modeling becomes much more complicated.

As it is known, in the type synthesis of lower-mobility parallel manipulators, particular geometric conditions are usually constructed to impose prescribed kinematic constraints to the moving platform. However, these conditions will be violated if geometric errors are taken into account. As a consequence, error models of these parallel manipulators are not easy to obtain from the nominal inverse kinematics directly. Hence, assumptions guaranteeing particular geometric conditions are usually made for the kinematic calibration of limited-DOF parallel manipulators.

Verner et al.[28] presented the kinematic calibration of a 3-PRS parallel manipulator under the assumption that the P and R joints are perpendicular to each other, which only requires one parameter to describe their relative position. Wang and Fan[29] neglected the errors between the axis of P joint and the base plate when established the error model of a 3-PRS serial–parallel machine tool. The error model of a 3-RPS parallel manipulator was established by Denavit-Hartenberg method and the cost functions were selected as the link length residuals, which means three more geometric constraints should be built up, otherwise not all of the kinematic parameters can be exactly identified.[30] To guarantee the 3-DOF translational mobility, Pashkevich et al.[31] assumed that the linear actuators are mutually orthogonal and intersected at a common point, namely the legs are strictly parallel to the corresponding Cartesian planes, in the kinematic calibration of orthoglide-type mechanisms. Gojtan et al.[32] analyzed the positioning accuracy of a 2-UPS-PRP parallel manipulator by assuming a perpendicular relation of joint axes in the PRP limbs. Similarly, Bai et al.[33] conducted the kinematic calibration of Delta parallel robot by assuming the traveling plate perfectly parallel to the base frame. Besides, in the kinematic calibration of planar parallel manipulators,[34–36] the error sources that violate the prescribed plane constraints of the mechanisms are usually neglected from the system for the sake of simplicity.

In this paper, a new kinematic calibration method is presented for the 3-PRS parallel manipulator based on the geometric constraint of limbs. Unlike existing ones depending on the manipulators' system error models, the proposed method takes advantage of geometric characteristics of the studied parallel manipulator and the kinematic parameters can be identified via two separated steps. In the first step, the spatial planes where the PRS limbs exactly located are determined through an

https://doi.org/10.1017/S0263574718001352 Published online by Cambridge University Press

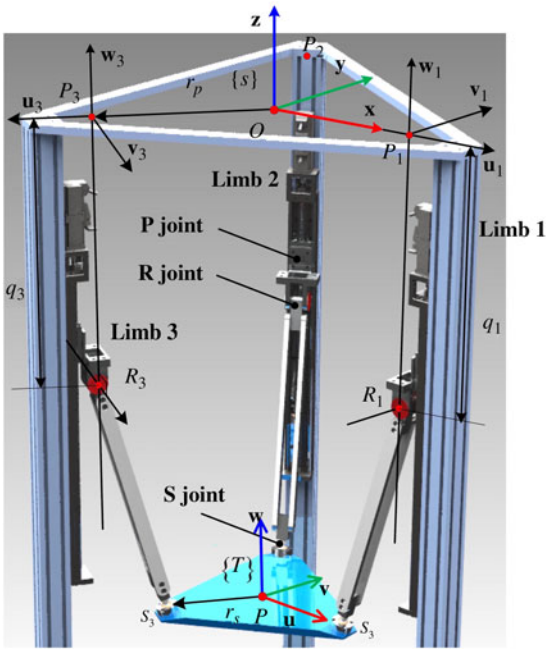

Fig. 1. Kinematic structure of the studied 3-PRS parallel manipulator.

optimization problem minimizing the residual distances of the spherical joints to these planes. As a consequence, the identification of limbs' kinematic parameters, which are considered as planar PR linkages, can be accomplished individually within the limb planes determined in the first step. The main advantage of the proposed method is the simplification of calibration modeling which does not require overall error models relating all kinematic errors to output ones. Instead, only two simple geometric problems need to be established for the planes of limbs and the axes of prismatic joints, successively. The effectiveness and efficiency of the proposed method have been validated via the calibration experiments on an apparatus of the 3-PRS parallel manipulator.

This paper is organized as follows: the schematic structure of the studied 3-PRS parallel manipulator is presented in Section 2, where the nominal inverse kinematics is also established. Then, Section 3 presents the error modeling of the proposed calibration method in detail, based on which the kinematic parameters can be identified via two simple geometric problems. To verify the correctness and efficiency of the proposed method, calibration experiments are conducted on the studied 3-PRS parallel manipulator in Section 4. In the end, some conclusions are drawn in Section 5.

2. Architecture and Kinematics of the Studied 3-PRS Parallel Manipulator

2.1. Architecture description

The studied 3-PRS parallel manipulator has a symmetric kinematic structure. Here, "P," "R," and "S' represent the prismatic, revolute, and spherical joints, respectively. And the underlined "P" means that the prismatic joint is actively actuated. As shown in Fig. 1, the P joints are vertically arranged, which form an equilateral triangle on the horizontal. In each limb, the axis of R joint is perpendicular to the corresponding P joint and parallel to the opposite side of the aforementioned triangle. The S joints on moving platform also locate at the vertices of an equilateral triangle.

As illustrated in the figure, the intersection points of P-joint with the horizontal plane are denoted by P_i, $i = 1, 2, 3$. Thus, $\Delta P_1 P_2 P_3$ is an equilateral triangle. The inertial frame of the parallel manipulator, denoted by $\{S\}$, is located at the center of $\Delta P_1 P_2 P_3$, namely the point O in the figure. The **z**-axis of $\{S\}$ is perpendicular to the triangle plane and the **x**-axis passes through P_1. Therefore, the position coordinates of P_i with respect to $\{S\}$ can be represented as

$$\mathbf{r}_{P_i} = r_p \, \mathbf{u}_i = \begin{bmatrix} r_p \, C_{\theta_i} \\ r_p \, S_{\theta_i} \\ 0 \end{bmatrix}, \quad i = 1, 2, 3 \tag{1}$$

https://doi.org/10.1017/S0263574718001352 Published online by Cambridge University Press

where r_p denotes the distance from the origin O to the prismatic joint, namely $\|OP_i\|$. $\theta_i = 2(i-1)\pi/3$ represent the directions of P joints. And $\mathbf{u}_i$ is the corresponding unit vector. C_{θ_i} and S_{θ_i} stand for $\cos\theta_i$ and $\sin\theta_i$, respectively.

Analogously, the tool frame $\{T\}$ is attached to the manipulator's moving platform at the center of the equilateral triangle $\Delta S_1S_2S_3$. Here, S_i, $i = 1, 2, 3$, denote the positions of spherical joints. Similar to $\{S\}$, $\mathbf{u}$-axis of $\{T\}$ passes through S_1 and $\mathbf{w}$-axis is perpendicular to the plane $\Delta S_1S_2S_3$. Thus, the coordinates of S_i in $\{T\}$ can be obtained as $\mathbf{s}_i = r_s\,\mathbf{u}_i$, where r_s is the distance from the origin P to S_i, namely $\|PS_i\|$.

Let $\mathbf{v}_i$ and $\mathbf{w}_i$ be the unit vectors associated with the axes of R and P joints, respectively. It is obvious that $\mathbf{v}_i$ is perpendicular to $\mathbf{r}_i$ and $\mathbf{w}_i$ is parallel to $\mathbf{z}$-axis of $\{S\}$ for all $i = 1, 2, 3$. Then, the position coordinates of R joint with respect to $\{S\}$ can be obtained as

$$\mathbf{r}_{R_i} = \mathbf{r}_{P_i} + q_i\,\mathbf{w}_i,\ i = 1, 2, 3 \tag{2}$$

where q_i, $i = 1, 2, 3$ represent the distances from the sliders to P_i, which are also considered as the input variables of the manipulator's active P joints.

Since the revolute joints are perpendicular to the corresponding prismatic ones, the position of the spherical joints is constrained on the vertical planes passing through O and P_i, denoted by $\mathscr{P}_i$. Obviously, the unit vector $\mathbf{v}_i$ just relates to the normal direction of $\mathscr{P}_i$.

2.2. Normal inverse kinematics analysis

As it is known, the moving platform of the studied 3-PRS parallel manipulator has two rotational and one translational DOFs. Simultaneously, parasitic motions of the moving platform will occur about the other 1-DOF rotation and 2-DOF translations. In other words, only three components of the manipulator's pose variables are independent, and the others should be determined according to them. Let α, β, and γ be the rotation angles about the $\mathbf{u}$, $\mathbf{v}$, and $\mathbf{w}$ axes of $\{T\}$. And let $\mathbf{p} = [x,\ y,\ z]^T$ be the relative position vector of $\{T\}$ with respect to $\{S\}$.

Let α, β, and z be the independent pose variables. Then, the others can be determined according to the geometric constraints of spherical joints on the corresponding limb planes, which can be represented as

$$\begin{cases} \mathbf{v}_1^T(\mathbf{r}_{S_1} - \mathbf{r}_{P_1}) = 0 \\ \mathbf{v}_2^T(\mathbf{r}_{S_2} - \mathbf{r}_{P_2}) = 0 \\ \mathbf{v}_3^T(\mathbf{r}_{S_3} - \mathbf{r}_{P_3}) = 0 \end{cases} \tag{3}$$

where $\mathbf{r}_{S_i} = \mathbf{R}\,\mathbf{s}_i + \mathbf{p}$ represents the position coordinates of spherical joints with respect to $\{S\}$. Here, $\mathbf{R}$ denotes the rotation matrix of $\{T\}$ relative to $\{S\}$, which can be expressed in terms of α, β, and γ as

$$\mathbf{R} = \mathrm{Rot}(\mathbf{u}, \alpha)\,\mathrm{Rot}(\mathbf{v}, \beta)\,\mathrm{Rot}(\mathbf{w}, \gamma) = \begin{bmatrix} C_\beta C_\gamma & -C_\beta S_\gamma & S_\beta \\ C_\alpha S_\gamma + S_\alpha S_\beta C_\gamma & C_\alpha C_\gamma - S_\alpha S_\beta S_\gamma & -S_\alpha C_\beta \\ S_\alpha S_\gamma - C_\alpha S_\beta C_\gamma & S_\alpha C_\gamma + C_\alpha S_\beta S_\gamma & C_\alpha C_\beta \end{bmatrix} \tag{4}$$

where $C_{(\cdot)} = \cos(\cdot)$ and $S_{(\cdot)} = \sin(\cdot)$ for $(\cdot)$ representing α, β, and γ.

Substituting Eq. (4) into Eq. (3), the parasitic motion variables can be derived analytically as

$$\begin{cases} \gamma = \arctan\dfrac{-S_\alpha\,S_\beta}{C_\alpha + C_\beta} \\ \begin{bmatrix} x \\ y \end{bmatrix} = \begin{bmatrix} \tilde{\mathbf{v}}_1^T \\ \tilde{\mathbf{v}}_2^T \end{bmatrix}^{-1} \begin{bmatrix} \mathbf{v}_1^T\,\mathbf{R}\,\mathbf{s}_1 \\ \mathbf{v}_2^T\,\mathbf{R}\,\mathbf{s}_2 \end{bmatrix} \end{cases} \tag{5}$$

where $\tilde{\mathbf{v}}_i = [-S_{\theta_i},\ C_{\theta_i}]^T$, $i = 1, 2$ is the vector comprising the first two components of $\mathbf{v}_i$.

According to Eq. (5), the pose of the end-effector can be determined once the independent pose variables α, β, and z are given. Then, the position coordinates of the spherical joints in $\{S\}$ can be derived accordingly, which specify the inputs of the active prismatic joints on the limb planes.

https://doi.org/10.1017/S0263574718001352 Published online by Cambridge University Press

According to Eq. (2), the input variables can be established according to the links' length constraints, which can be represented in the form of quadratic equations as

$$\|\mathbf{r}_{R_i} - \mathbf{r}_{S_i}\|^2 = (q_i \mathbf{w}_i + \mathbf{r}_{P_i} - \mathbf{r}_{S_i})^T (q_i \mathbf{w}_i + \mathbf{r}_{P_i} - \mathbf{r}_{S_i}) = l_i^2, \quad i = 1, 2, 3 \tag{6}$$

where l_i denotes the length of the limb's link.

Solving Eq. (6), the closed-form solution to the input variable q_i can be obtained readily as

$$q_i = -\mathbf{w}_i^T (\mathbf{r}_{P_i} - \mathbf{r}_{S_i}) - \sqrt{l_i^2 - \|\mathbf{r}_{P_i} - \mathbf{r}_{S_i}\|^2 + |\mathbf{w}_i^T (\mathbf{r}_{P_i} - \mathbf{r}_{S_i})|^2}, \quad i = 1, 2, 3 \tag{7}$$

where $\mathbf{w}_i^T (\mathbf{r}_{P_i} - \mathbf{r}_{S_i})$ denotes the projective distance of $P_i S_i$ on the corresponding prismatic joint, and $\|\mathbf{r}_{P_i} - \mathbf{r}_{S_i}\|$ relates to the distance between $\mathbf{r}_{S_i}$ and $\mathbf{r}_{P_i}$. Here, it should be noted that there exist two different solutions for each $q_i, i = 1, 2, 3$. And they correspond to different assembling configurations of the limbs. In the above equation, the improper solution to the studied manipulator is eliminated for the sake of simplification.

According to Eq. (7), for a given pose of the manipulator's end-effector, the required input variables of the active prismatic joints can be derived in a straightforward way. However, due to the manufacturing/assembling tolerances, there exists a deviation between the actual values of the manipulator's kinematic parameters and their nominal ones. In order to minimize the influence of those errors on the positioning accuracy, kinematic calibration should be carried out on the parallel manipulator to compensate these errors by means of using the identified kinematic parameters in the control algorithm.

3. Error Modeling of the Proposed Two-Step Approach

In conventional kinematic calibration approaches, an overall error model which comprises all kinematic errors is usually established for iterative identification of the manipulator's kinematic parameters. In this section, a two-step identification approach is proposed for the kinematic calibration of the studied 3-PRS parallel manipulator by taking advantage of the limbs' geometric constraints.

3.1. Identification of the positions of spherical joints and limb planes

As indicated in the above section, the position of spherical joints on the moving platform is constrained on the corresponding limb plane $\mathscr{P}_i$. Ideally, these planes are vertical ones and commonly intersected at the **z**-axis of $\{S\}$. But in practice, their poses (position and orientation) will be deviated from the nominal ones due to kinematic errors. Hence, in the proposed calibration method, the exact poses of these limb planes are identified in the first step.

Let $\mathbf{n}_i$ be the unit normal vector of $\mathscr{P}_i$ and d_i the directional distance from the origin O to $\mathscr{P}_i$. Then, the position of plane can be represented by the projection point of O on $\mathscr{P}_i$, which is denoted by O_i as illustrated in Fig. 2. Thus, the position vector of O_i in $\{S\}$ can be obtained directly as $\mathbf{r}_{O_i} = d_i \mathbf{n}_i$. And the distance from the spherical joint S_i to the corresponding limb plane $\mathscr{P}_i$ can be derived as

$$y_i = \mathbf{n}_i^T (\mathbf{r}_{S_i} - \mathbf{r}_{O_i}) = \mathbf{n}_i^T \mathbf{R}\, \mathbf{s}_i + \mathbf{n}_i^T \mathbf{p} - d_i, \quad i = 1, 2, 3 \tag{8}$$

It is worth noting that the distance (8) should be zero in the case of the manipulator's nominal kinematics as indicated in Eq. (3). However, due to the position error of the spherical joints and those of the limb planes, the calculated distance y_i according to the measured configurations of moving platform will not vanish using the nominal kinematic errors. Therefore, the identification problem can be transformed to find the best values of the parameters $\mathbf{n}_i$, $\mathbf{s}_i$, and d_i to minimize y_i for all measured configurations.

It should be noted that the position $\mathbf{p}$ and orientation $\mathbf{R}$ of the manipulator's tool frame $\{T\}$ are directly measured using an external pose sensor. Since the measurement noise is not taken into account, $\mathbf{p}$ and $\mathbf{R}$ are considered as accurate variables in proposed calibration method. Hence, Gauss-Newton algorithm can be used to identify the best solutions of those kinematic parameters, and the objective function can be described as

$$\min \left| \mathbf{n}_i^T \mathbf{R}\, \mathbf{s}_i + \mathbf{n}_i^T \mathbf{p} - d_i \right|, \quad i = 1, 2, 3 \tag{9}$$

https://doi.org/10.1017/S0263574718001352 Published online by Cambridge University Press

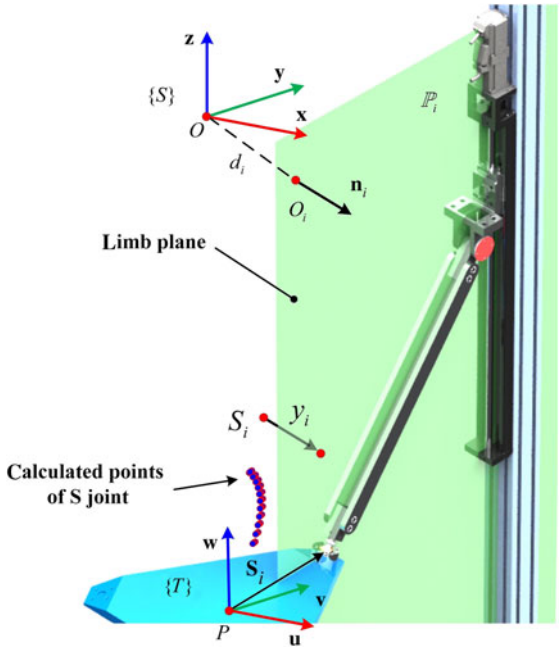

Fig. 2. Identification of the spatial planes for the PRS limbs.

Let $\mathbf{p}_j$ and $\mathbf{R}_j$, $j = 1, \cdots, m$, be the position and orientation of $\{S\}$ associated with the jth measurement. Then, the gradient equation of (8) can be obtained as

$$\delta y_{i,j} = \mathbf{n}_i^T \mathbf{R}_j \, \delta \mathbf{s}_i + (\mathbf{R}_j \, \mathbf{s}_i + \mathbf{p}_j)^T \delta \mathbf{n}_i - \delta d_i = \mathbf{J}_{\mathbf{p}_{i,j}} \, \delta \mathbf{p}_i, \;\; i = 1, 2, 3; \;\; j = 1, \cdots, m \tag{10}$$

where $\mathbf{J}_{\mathbf{p}_{i,j}} = [\mathbf{n}_i^T \mathbf{R}_j, \, (\mathbf{R}_j \, \mathbf{s}_i + \mathbf{p}_j)^T, \, -1] \in \mathbb{R}^{1\times 7}$ can be regarded as the sensitivity matrix of the geometric parameters on the unexpected distance between the corresponding S joint and limb plane. $\mathbf{p}_i = \left[\mathbf{s}_i^T, \; \mathbf{n}_i^T, \; d_i\right]^T \in \mathbb{R}^{7\times 1}$ is the column vector consisting of the limb's kinematic parameters.

Equation (10) relates to a general optimization problem; the unknown variables $\mathbf{p}_i$ can be determined by gradient-based searching algorithm. Therefore, the iterative update theme can be established readily by means of assembling all configuration measurements together, as

$$\delta \mathbf{y}_i = \begin{bmatrix} \delta y_{i,1} \\ \vdots \\ \delta y_{i,m} \end{bmatrix} = \begin{bmatrix} \mathbf{J}_{\mathbf{p}_{i,1}} \\ \vdots \\ \mathbf{J}_{\mathbf{p}_{i,m}} \end{bmatrix} \delta \mathbf{p}_i = \mathbf{J}_{\mathbf{p}_i} \, \delta \mathbf{p}_i \Rightarrow \mathbf{p}_i^{k+1} = \mathbf{p}_i^k + \left(\mathbf{J}_{\mathbf{p}_i}^T \mathbf{J}_{\mathbf{p}_i}\right)^{-1} \mathbf{J}_{\mathbf{p}_i}^T \delta \mathbf{y}_i^k, \;\; i = 1, 2, 3 \tag{11}$$

where the superscript k means the kth iteration of the searching algorithm.

According to Eq. (11), the kinematic parameter $\mathbf{p}_i$ will be repeatedly updated until $\delta \mathbf{p}_i$ approaches zero and the residual distance $\mathbf{y}_i$ converges to some stable value. According to the identified values of $\mathbf{s}_i$, $\mathbf{n}_i$, and d_i, the actual positions of spherical joints on the moving platform and the corresponding poses of limb planes can be specified conveniently.

3.2. Identification of the limb parameters

As indicated in Section 3.1, in the first step, the position of S-joint and limb plane has been identified according to the geometric constraints. Thus, the identification of the prismatic joints and the link lengths can be accomplished by considering the kinematic limbs as planar PR linkages on the corresponding limb planes.

As shown in Fig. 3, the projection of P_i on $\mathscr{P}_i$, denoted by Q_i, is employed to construct the limb's local frame. Let $\{O_i\}$ be the local frame whose origin coincides with O_i and $\mathbf{x}_i$-axis passes through Q_i. The $\mathbf{z}_i$-axis of $\{O_i\}$ is parallel to normal vector of $\mathscr{P}_i$, namely the identified unit vector $\mathbf{n}_i$.

https://doi.org/10.1017/S0263574718001352 Published online by Cambridge University Press

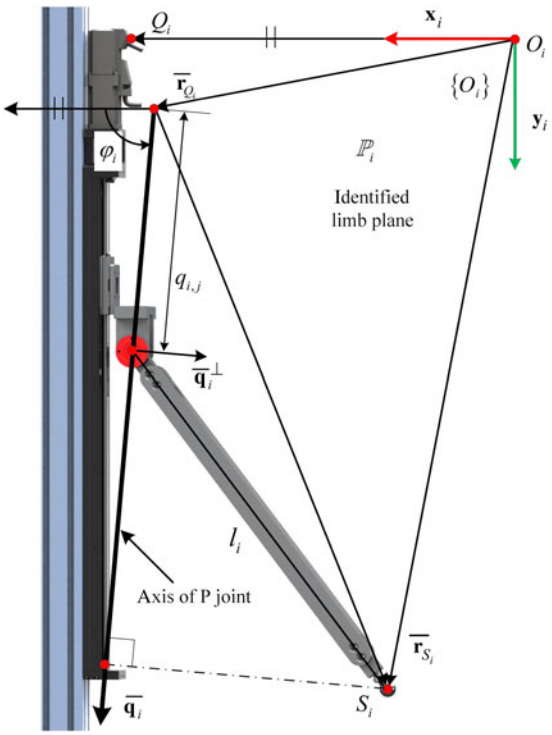

Fig. 3. Identification of limb parameters within the identified plane.

And the $\mathbf{y}_i$-axis is specified according to the right-hand rule. As a result, the relative position and orientation of the local frame $\{O_i\}$ with respect to $\{S\}$ can be obtained as

$$\mathbf{o}_i = d_i\,\mathbf{n}_i,\ \mathbf{R}_i = \left[\mathbf{x}_i,\ \mathbf{y}_i,\ \mathbf{z}_i\right],\ \ i = 1, 2, 3 \tag{12}$$

where $\mathbf{x}_i = \frac{1}{\left\|\left(\mathbf{I}_3 - \mathbf{n}_i\mathbf{n}_i^T\right)\mathbf{r}_{P_i}\right\|}\left(\mathbf{I}_3 - \mathbf{n}_i\mathbf{n}_i^T\right)\mathbf{r}_{P_i}$, $\mathbf{z}_i = \mathbf{n}_i$, and $\mathbf{y}_i = \mathbf{z}_i \times \mathbf{x}_i$. $\mathbf{I}_3$ is the three-order identity matrix.

Let Q_i be the initial position of prismatic joint and $\mathbf{q}_i$ be its axis direction. Then, the cost function of the limb's kinematic errors can be constructed as the deviation of link length of the form

$$c_i = \left\|\overline{\mathbf{r}}_{Q_i} + q_i\,\overline{\mathbf{q}}_i - \overline{\mathbf{r}}_{S_i}\right\| - l_i,\ \ i = 1, 2, 3 \tag{13}$$

where $\overline{\mathbf{r}}_{Q_i}$ and $\overline{\mathbf{r}}_{S_i}$ are planar coordinates of Q_i and S_i, respectively, with respect to the local frame $\{O_i\}$. $\overline{\mathbf{q}}_i = [C_{\varphi_i},\ S_{\varphi_i}]^T$ represents the direction of prismatic joint in $\{O_i\}$ with the directional angle φ_i. And l_i is link length in the limb.

Theoretically, the cost function (13) should be equal to 0 for all limbs using the measured configurations. However, in practice, there exist a deviation of the actual values from the nominal ones due to the manipulator's kinematic errors. In this problem, $\overline{\mathbf{r}}_{S_i}$ and q_i can be considered as measured variables without noise errors. Hence, the identification problem can be stated as to find the best $\overline{\mathbf{r}}_{Q_i}$, φ_i, and l_i to minimize c_i for all measurements. The gradient function of (13) can be derived as

$$\delta c_{i,j} = \frac{\left(\overline{\mathbf{r}}_{Q_i} + q_{i,j}\,\overline{\mathbf{q}}_i - \overline{\mathbf{r}}_{S_{i,j}}\right)^T}{\left\|\overline{\mathbf{r}}_{Q_i} + q_{i,j}\,\overline{\mathbf{q}}_i - \overline{\mathbf{r}}_{S_{i,j}}\right\|}\left(\delta\overline{\mathbf{r}}_{Q_i} + q_{i,j}\,\overline{\mathbf{q}}_i^{\perp}\delta\varphi_i\right) - \delta l_i = \mathbf{J}_{L_{i,j}}\delta\mathbf{p}_{L_i},\ \ i = 1, 2, 3;\ \ j = 1, \ldots, m \tag{14}$$

where $\delta\overline{\mathbf{q}}_i = [-S_{\varphi_i},\ C_{\varphi_i}]^T\,\delta\varphi_i = \overline{\mathbf{q}}_i^{\perp}\delta\varphi_i$ denotes the planar unit vector perpendicular to $\overline{\mathbf{q}}_i$. $\mathbf{p}_{L_i} = \left[\overline{\mathbf{r}}_{Q_i},\ \varphi_i,\ l_i\right]^T \in \mathbb{R}^{4\times 1}$ is the limb's kinematic parameters and $\mathbf{J}_{L_{i,j}} = \left[\frac{(\overline{\mathbf{r}}_{Q_i} + q_{i,j}\,\overline{\mathbf{q}}_i - \overline{\mathbf{r}}_{S_{i,j}})^T}{\|\overline{\mathbf{r}}_{Q_i} + q_{i,j}\,\overline{\mathbf{q}}_i - \overline{\mathbf{r}}_{S_{i,j}}\|},\ \frac{q_{i,j}(\overline{\mathbf{r}}_{Q_i} + q_{i,j}\,\overline{\mathbf{q}}_i - \overline{\mathbf{r}}_{S_{i,j}})^T\overline{\mathbf{q}}_i^{\perp}}{\|\overline{\mathbf{r}}_{Q_i} + q_{i,j}\,\overline{\mathbf{q}}_i - \overline{\mathbf{r}}_{S_{i,j}}\|},\ -1\right] \in \mathbb{R}^{1\times 4}$ is the corresponding sensitivity matrix.

According to Eq. (14), it is known that in each limb there are four kinematic parameters to be identified, namely $\overline{\mathbf{r}}_{Q_i}$, φ_i, and l_i. From geometric point of view, they correspond to the position and

https://doi.org/10.1017/S0263574718001352 Published online by Cambridge University Press

direction of prismatic joint on the limb plane, and the length of link, respectively. Using the same theme as in Eq. (11), the gradient-based searching algorithm can be iteratively repeated according to

$$\delta \mathbf{c}_i = \begin{bmatrix} \delta c_{i,1} \\ \vdots \\ \delta c_{i,m} \end{bmatrix} = \begin{bmatrix} \mathbf{J}_{L_{i,1}} \\ \vdots \\ \mathbf{J}_{L_{i,m}} \end{bmatrix} \delta \mathbf{p}_{L_i} = \mathbf{J}_{L_i}\, \delta \mathbf{p}_{L_i} \Rightarrow \mathbf{p}_{L_i}^{k+1} = \mathbf{p}_{L_i}^{k} + \left(\mathbf{J}_{\mathbf{L}_i}^T \mathbf{J}_{\mathbf{L}_i}\right)^{-1} \mathbf{J}_{\mathbf{L}_i}^T \delta \mathbf{c}_i^k, \;\; i = 1, 2, 3 \tag{15}$$

where the identification matrix can be obtained readily as $\mathbf{J}_{\mathbf{L}_i} = \left[\mathbf{J}_{L_{i,1}}^T, \cdots, \mathbf{J}_{L_{i,m}}^T\right]^T \in \mathbb{R}^{m\times 4}$.

Analogous to the first step indicated in Section 3.1, the actual values of the prismatic joints' positions and the lengths of links can be identified when the searching algorithm (15) converses to stable values. Then, the coordinates of the identified vector $\bar{\mathbf{r}}_{Q_i}$ and $\bar{\mathbf{q}}_i$ can be transformed from $\{O_i\}$ to $\{S\}$ as

$$\mathbf{r}_{Q_i} = \mathbf{o}_i + \mathbf{R}_i\, \bar{\mathbf{r}}_{Q_i}, \;\; \mathbf{q}_i = \mathbf{R}_i\, \bar{\mathbf{q}}_i, \;\; i = 1, 2, 3 \tag{16}$$

where $\mathbf{R}_i$ and $\mathbf{o}_i$ are defined in Eq. (12).

With this, all kinematic parameters of the studied 3-PRS parallel manipulator have been identified and represented with respect to the system inertial frame. Thereinto, $\mathbf{r}_{Q_i}$ and $\mathbf{q}_i$ specify the position and direction of the prismatic joint. l_i denotes the link length in the limb. $\mathbf{n}_i$ and d_i determine the direction and position of the corresponding limb plane. And $\mathbf{s}_i$ is the position coordinates of spherical joint with respect to $\{T\}$.

3.3. Actual inverse kinematics of the 3-PRS parallel manipulator

In order to increase the positioning accuracy of the studied 3-PRS parallel manipulator, the inaccurate kinematics should be corrected in terms of the identified parameters in the above two steps. The required inputs of prismatic joints can be determined by means of two steps according to the actual geometric constraints of the parallel manipulator.

Since the actual limb planes are not vertically intersected at the **z**-axis of $\{S\}$ any more, the geometric constraints of the moving platform's spherical joints (3) should be modified as

$$\mathbf{n}_i^T (\mathbf{R}\, \mathbf{s}_i + \mathbf{p} - d_i\, \mathbf{n}_i) = 0 \Rightarrow \mathbf{n}_i^T \mathbf{R}\, \mathbf{s}_i + \mathbf{n}_i^T \mathbf{p} = d_i, \;\; i = 1, 2, 3 \tag{17}$$

Since α, β, and z are independent pose variables of the manipulator's moving platform, the geometric constraint equation (17) can be rewritten as

$$\begin{bmatrix} n'_{11}s_{11} + n'_{12}s_{12} \\ n'_{21}s_{21} + n'_{22}s_{22} \\ n'_{31}s_{31} + n'_{32}s_{32} \end{bmatrix} \cos\gamma + \begin{bmatrix} n'_{12}s_{11} - n'_{11}s_{12} \\ n'_{22}s_{21} - n'_{21}s_{22} \\ n'_{32}s_{31} - n'_{31}s_{32} \end{bmatrix} \sin\gamma + \begin{bmatrix} n_{11} & n_{12} \\ n_{21} & n_{22} \\ n_{31} & n_{32} \end{bmatrix} \begin{bmatrix} x \\ y \end{bmatrix} = \begin{bmatrix} d_1 - n'_{13}s_{13} - n_{13}z \\ d_2 - n'_{23}s_{23} - n_{23}z \\ d_3 - n'_{33}s_{33} - n_{33}z \end{bmatrix} \tag{18}$$

where $\mathbf{n}_i = [n_{i,1},\ n_{i,2},\ n_{i,3}]^T$ and $\mathbf{s}_i = [s_{i,1},\ s_{i,2},\ s_{i,3}]^T$ and $\mathbf{n}'_i = [n'_{i,1}, n'_{i,2}, n'_{i,3}]^T = \mathrm{Rot}(\mathbf{v}, \beta)^T \mathrm{Rot}(\mathbf{u}, \alpha)^T \mathbf{n}_i$.

Let $\boldsymbol{\lambda} = [\lambda_1,\ \lambda_2,\ \lambda_3]^T$ be the unit vector satisfying $\lambda_1 n_{11} + \lambda_2 n_{21} + \lambda_3 n_{31} = 0$ and $\lambda_1 n_{12} + \lambda_2 n_{22} + \lambda_3 n_{32} = 0$. Then, pre-multiplying (18) with $\boldsymbol{\lambda}^T$, the dependent variable γ can be derived as

$$A_\gamma\, \cos\gamma + B_\gamma\, \sin\gamma = D_\gamma \Rightarrow \gamma = \arcsin \frac{D_\gamma}{\sqrt{A_\gamma^2 + B_\gamma^2}} - \arctan \frac{A_\gamma}{B_\gamma} \tag{19}$$

where the scalar coefficients are given by

$$\begin{cases} A_\gamma = \left(n'_{11}s_{11} + n'_{12}s_{12}\right)\lambda_1 + \left(n'_{21}s_{21} + n'_{22}s_{22}\right)\lambda_2 + \left(n'_{31}s_{31} + n'_{32}s_{32}\right)\lambda_3 \\ B_\gamma = \left(n'_{12}s_{11} - n'_{11}s_{12}\right)\lambda_1 + \left(n'_{22}s_{21} - n'_{21}s_{22}\right)\lambda_2 + \left(n'_{32}s_{31} - n'_{31}s_{32}\right)\lambda_3 \\ D_\gamma = \boldsymbol{\lambda}^T \mathbf{d} - \left(n'_{13}s_{13} + n_{13}z\right)\lambda_1 - \left(n'_{23}s_{23} + n_{23}z\right)\lambda_2 - \left(n'_{33}s_{33} + n_{33}z\right)\lambda_3 \end{cases}$$

where $\mathbf{d} = [d_1,\ d_2,\ d_3]^T$.

https://doi.org/10.1017/S0263574718001352 Published online by Cambridge University Press

Table I. The nominal kinematic parameters of the 3-PRS prototype (unit: m/rad).

Limbs no.	$\mathbf{r}_{P_i}$	$\mathbf{r}_{S_i}$	$\boldsymbol{V}_i$
1	$[\,0.3140,\ 0.0000,\ 0.0000\,]^T$	$[-0.1705,\ 0.2953,\ 0.0000\,]^T$	$[-0.1705,\ 0.2953,\ 0.0000\,]^T$
2	$[\,0.2000,\ 0.0000,\ 0.0000\,]^T$	$[-0.1000,\ 0.1732,\ 0.0000\,]^T$	$[-0.1000,\ -0.1732,\ 0.0000\,]^T$
3	$[\,0.0000,\ 1.0000,\ 0.0000\,]^T$	$[-0.8660,\ -0.5000,\ 0.0000\,]^T$	$[\ 0.8660,\ -0.5000,\ 0.0000\,]^T$

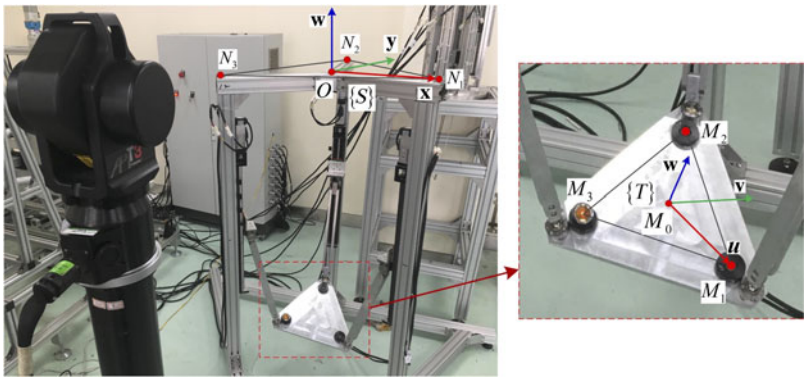

Fig. 4. Experimental apparatus for the kinematic calibration of the 3-PRS parallel manipulator.

Substituting Eq. (19) into Eq. (17), the position vector can be derived as

$$\mathbf{p} = \begin{bmatrix} \mathbf{n}_1^T \\ \mathbf{n}_2^T \\ \mathbf{n}_3^T \end{bmatrix}^{-1} \begin{bmatrix} d_1 - \mathbf{n}_1^T \mathbf{R}\,\mathbf{s}_1 \\ d_2 - \mathbf{n}_2^T \mathbf{R}\,\mathbf{s}_2 \\ d_3 - \mathbf{n}_3^T \mathbf{R}\,\mathbf{s}_3 \end{bmatrix} \tag{20}$$

According to Eqs. (19) and (20), the actual pose of the manipulator's tool frame $\{T\}$ can be uniquely obtained in terms of the independent variables α, β, and z, so are the corresponding position vectors of spherical joints. Then, the input variables of the prismatic joints can be derived as

$$q_i = \mathbf{q}_i^T(\mathbf{r}_{S_i} - \mathbf{r}_{Q_i}) + \sqrt{l_i^2 - \|\mathbf{r}_{S_i} - \mathbf{r}_{Q_i}\|^2 + |\mathbf{q}_i^T(\mathbf{r}_{S_i} - \mathbf{r}_{Q_i})|^2} \tag{21}$$

where $\mathbf{r}_{S_i} = \mathbf{R}\,\mathbf{s}_i + \mathbf{p}$ denotes the actual position of spherical joint according to the identified parameters.

Comparing Eqs. (19)–(21) with Eqs. (5) and (7), it is known that the solving strategy of the parallel manipulator's actual kinematics is as same as the nominal one. The difference is caused by the misalignment of the manipulator's limb planes due to kinematic errors, namely $\mathbf{n}_i \neq \mathbf{u}_i$ and $d_i \neq 0$. Therefore, the inverse kinematics solution in the control theme should be corrected by the actual ones in terms of the identified parameters.

4. Experimental Validation

In this section, an experimental apparatus was built up to validate the effectiveness and efficiency of the proposed two-step method for kinematic calibration of the studied 3-PRS parallel manipulator. The results show that the iterative searching algorithms converge quickly for both identification steps, and the positioning accuracy of the manipulator has been significantly improved using the identified kinematic parameters.

The radii of the fixed and moving platforms' circumcircles r_p and r_s of the 3-PRS prototype are designed as 0.314 and 0.2 m, respectively, and the length of the links l_i is 0.514 m. According to these important structure parameters, the other kinematic parameters can then be determined and are listed in Table I. Besides, considering the rotation ability of the used spherical joints, the orientation workspaces of this manipulator about u and v axes are about $[-\pi/6,\ \pi/6]$ rad. As shown in Fig. 4, a

https://doi.org/10.1017/S0263574718001352 Published online by Cambridge University Press

high-precision laser tracker (API T3) is used to measure the configurations of the parallel manipulator's moving platform. According to the user manual of the laser tracker, the measurement accuracy is about 5 μm/m. As illustrated in the figure, three spherically mounted reflectors (SMRs) attached on the moving platform are measured to construct the manipulator's tool frame $\{T\}$. The positions of the measured points are denoted by $\mathbf{r}_{M_i}$, $i = 1, 2, 3$. The origin of $\{T\}$, denoted by M_0, is located at the center of $\Delta M_1 M_2 M_3$. Meanwhile, the $\mathbf{u}$-axis of $\{T\}$ is set to pass through M_1 and the $\mathbf{w}$-axis keep perpendicular to the plane $M_1 M_2 M_3$. On the other hand, three SMRs, denoted by N_i, $i = 1, 2, 3$, are attached on the fixed frame to construct the inertial frame $\{S\}$ in a similar way as $\{T\}$. The origin of $\{S\}$, denoted by O, is located at the center of $\Delta N_1 N_2 N_3$. The $\mathbf{z}$-axis keeps perpendicular to $N_1 N_2 N_3$ plane and the $\mathbf{x}$-axis passes through N_1. The $\mathbf{y}$-axis is specified as $\mathbf{y} = \mathbf{z} \times \mathbf{x}$.

It should be noted that the tool frame established according to the SMRs is slightly different from the ideal one by the three spherical joints on the moving platform. As a matter of fact, the manipulator's tool frame $\{T\}$ is a virtual coordinate frame and can be arbitrarily constructed as long as attaching to the moving platform. For the sake of simplification in kinematics modeling, it is located at the geometric center of the spherical joints on the moving platform. Thus, the spherical joints are equally distributed on a circle on the uv-plane of $\{T\}$ and centered at the origin. In the experimental validation, the physical centers of the spherical joints cannot be measured by the laser tracker. Hence, the tool frame $\{T\}$ was reconstructed in terms of the positions of the SMRs, namely the three black magnetic bases (M_1, M_2, and M_3). In such a scenario, the pose of the moving platform is represented by the reconstructed tool frame, rather than the nominal virtual one. As well, the position vectors of the spherical joints, namely s_i, $i = 1, 2, 3$, are also expressed with respect to the measured tool frame. Similarly, the pose of the fixed base is also represented by the reconstructed frame in terms of N_1, N_2, and N_3, rather than the nominal S. Besides, the three SMRs on the moving platform are very close to the three spherical joints, respectively. Thus, the pose deviation of the measured tool frame is not very large from the nominal one. Besides, since all the identified parameters are represented with respect to the measured tool frame, rather than the nominal one in kinematics analysis, the deviations between the measured and nominal frames only cause a rigid transformation of kinematic parameters between different reference frames, which does not influence the identification accuracy.

Then, the relative pose of the tool frame $\{T\}$ with respect to the system's inertial one $\{S\}$ can be obtained as

$$\mathbf{g}_{st} = \begin{bmatrix} \mathbf{R}_{st} & \mathbf{p}_{st} \\ \mathbf{0} & 1 \end{bmatrix} = \begin{bmatrix} \mathbf{R}_s & \mathbf{p}_s \\ \mathbf{0} & 1 \end{bmatrix}^{-1} \begin{bmatrix} \mathbf{R}_t & \mathbf{p}_t \\ \mathbf{0} & 1 \end{bmatrix} = \begin{bmatrix} \mathbf{R}_s^T \mathbf{R}_t & \mathbf{R}_s^T (\mathbf{r}_P - \mathbf{r}_O) \\ \mathbf{0} & 1 \end{bmatrix} \tag{22}$$

where $\mathbf{R}_s \in SO(3)$ and $\mathbf{r}_O \in \mathbb{R}^{3\times 1}$ are the rotation matrix and position vector of $\{S\}$ with respect to to the measurement coordinate frame. Accordingly, $\mathbf{R}_t$ and $\mathbf{r}_P$ are those of $\{T\}$.

The poses of $\{T\}$ and $\{S\}$ can be obtained in terms of the measured positions as

$$\begin{cases} \mathbf{r}_P = \dfrac{1}{3}\left(\mathbf{r}_{M_1} + \mathbf{r}_{M_2} + \mathbf{r}_{M_3}\right) \\ \mathbf{R}_t = [\,\mathbf{u},\ \mathbf{v},\ \mathbf{w}\,] \\ \mathbf{u} = \dfrac{1}{\|\mathbf{r}_{M_1} - \mathbf{r}_P\|}\left(\mathbf{r}_{M_1} - \mathbf{r}_P\right) \\ \mathbf{w} = \dfrac{(\mathbf{r}_{M_2} - \mathbf{r}_{M_1}) \times (\mathbf{r}_{M_3} - \mathbf{r}_{M_2})}{\|(\mathbf{r}_{M_2} - \mathbf{r}_{M_1}) \times (\mathbf{r}_{M_3} - \mathbf{r}_{M_2})\|} \\ \mathbf{v} = \mathbf{w} \times \mathbf{u} \end{cases} \quad \begin{cases} \mathbf{r}_O = \dfrac{1}{3}\left(\mathbf{r}_{N_1} + \mathbf{r}_{N_2} + \mathbf{r}_{N_3}\right) \\ \mathbf{R}_s = [\mathbf{x},\ \mathbf{y},\ \mathbf{z}] \\ \mathbf{x} = \dfrac{1}{\|\mathbf{r}_{N_1} - \mathbf{r}_O\|}\left(\mathbf{r}_{N_1} - \mathbf{r}_O\right) \\ \mathbf{z} = \dfrac{(\mathbf{r}_{N_2} - \mathbf{r}_{N_1}) \times (\mathbf{r}_{N_3} - \mathbf{r}_{N_2})}{\|(\mathbf{r}_{N_2} - \mathbf{r}_{N_1}) \times (\mathbf{r}_{N_3} - \mathbf{r}_{N_2})\|} \\ \mathbf{y} = \mathbf{z} \times \mathbf{x} \end{cases} \tag{23}$$

where $\mathbf{r}_{M_i}$ and $\mathbf{r}_{N_i}$ $(i = 1, 2, 3)$ are the measured positions of the corresponding SMRs.

To obtain sufficient configurations for the identification and validation, the manipulator's input of each limb is discretized for measurements. The initial pose of the manipulator is firstly determined when all the prismatic joints are at their midpoints. On this basis, the ranges of the inputs of the prismatic joints are set to $[-75, 75]$ mm, which is discretized by 30 mm. Thus, totally 216 configurations

https://doi.org/10.1017/S0263574718001352 Published online by Cambridge University Press

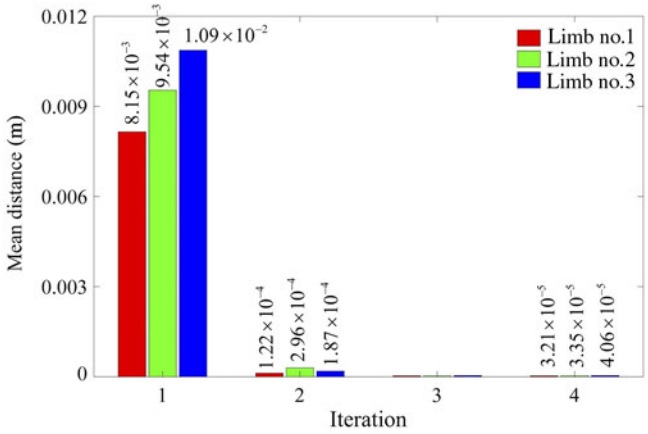

Fig. 5. Mean distances of the spherical joints to the corresponding limb planes during the first step identification.

are measured for the kinematic calibration of the 3-PRS parallel manipulator. And the inputs for each pose can be given as

$$\mathbf{g}_{st,\,n} \Rightarrow \begin{cases} q_1 = -75 + (i-1) \times 30 \\ q_2 = -75 + (j-1) \times 30 \\ q_3 = -75 + (k-1) \times 30 \end{cases}, \quad i = 1, \ldots, 6, \quad j = 1, \ldots, 6, \quad k = 1, \ldots, 6 \tag{24}$$

where $n = (i-1) \times 36 + (j-1) \times 6 + k = 1, \ldots, 216$ denotes the sequence number of measurements.

Then, the corresponding pose can be obtained readily according to the nominal forward kinematics. By means of measuring the mounted SMRs for each configuration, the actual values of the prescribed 216 poses can be derived according to Eqs. (22) and (23). As a result, the identification process for the manipulator's kinematic parameters can be carried out in terms of the corresponding input–output measurements. Among these measured configurations, 108 are chosen for the two-step identification of the kinematic parameters, while the other 108 are utilized for the validation of calibration result. Figure 5 illustrates the mean distances of the spherical joints to the corresponding limb planes during the iterative identification process. From the results, it is known that the initial distances are relatively large, due to the inaccuracy of the parameters' nominal values. Using the proposed gradient-based searching algorithm (11), the identification quickly (within four iterations) converges to some stable values and the residual distances have been significantly reduced to small values less than 5×10^{-5} m.

As mentioned above, there exists a specific shift of the spherical joints along the **w**-axis of $\{T\}$. This issue is caused by the distance between the planes of spherical joints and measured SMRs. As shown in Fig. 4, the centers of SMRs are higher than those of spherical joints, and this distances have been identified as about 0.024 m in the first-step calibration.

According to the identified parameters in the first step, the second step of the proposed calibration approach can be performed by following the procedures presented in Section 3.2. The mean length residuals (13) of the limbs' links are illustrated in Fig. 6 during the identification process. From the figure, it is known that the mean residuals quickly converge to some stable values around 2×10^{-4} m.

To verify the correctness of the proposed two-step calibration method, the rest 108 measured configurations, except for the above 108 for parameter identification, are used to compare the manipulator's positioning accuracy before and after calibration. It should be noted that a numerical algorithm is utilized to calculate the forward kinematics of the studied 3-PRS parallel manipulator in terms of the identified parameters. The position and orientation errors of validation configuration can then be calculated by the results of the forward kinematics and the measured pose. Let $[x_{c,i},\ y_{c,i}\ , z_{c,i},\ \alpha_{c,i},\ \beta_{c,i},\ \gamma_{c,i}]^T$ and $[x_{a,i},\ y_{a,i}\ , z_{a,i},\ \alpha_{a,i},\ \beta_{a,i},\ \gamma_{a,i}]^T$ denote the calculated and measured poses of the ith validation configuration; the position and orientation errors are described as

$$\begin{aligned} \delta p_i &= |[x_{c,i},\ y_{c,i}\ , z_{c,i}]^T - [x_{a,i},\ y_{a,i}\ , z_{a,i}]^T| \\ \delta r_i &= |[\alpha_{c,i},\ \beta_{c,i},\ \gamma_{c,i}]^T - [\alpha_{a,i},\ \beta_{a,i},\ \gamma_{a,i}]^T| \end{aligned} \tag{25}$$

https://doi.org/10.1017/S0263574718001352 Published online by Cambridge University Press

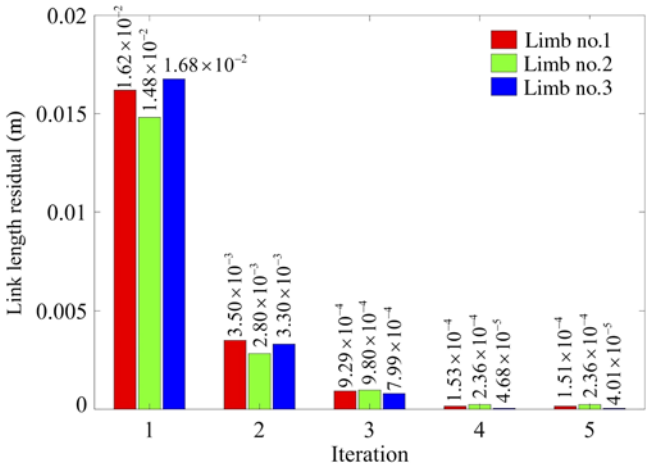

Fig. 6. Mean length residual of the limbs' links during the second step identification.

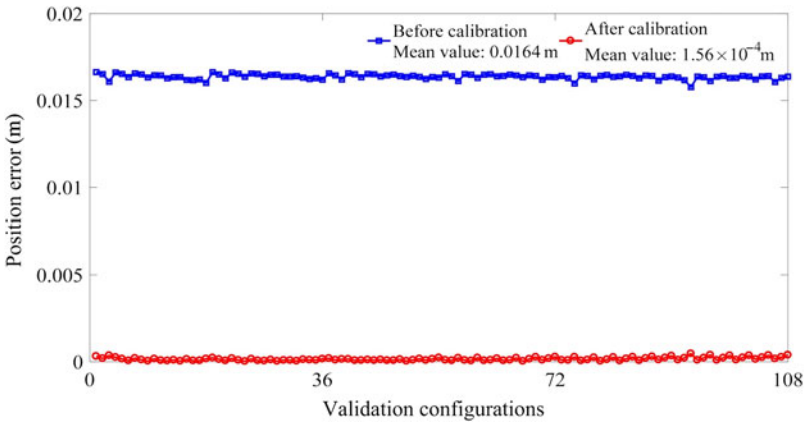

Fig. 7. Position errors of the validation configurations.

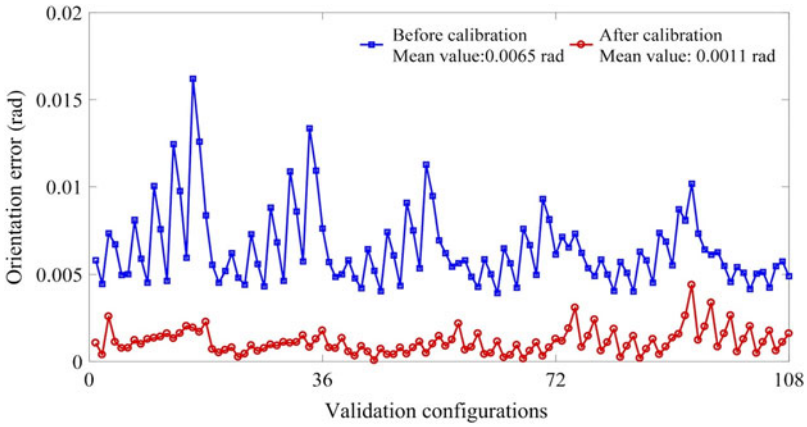

Fig. 8. Orientation errors of the validation configurations.

The residual position and orientation errors of the validation configurations are drawn in Figs. 7 and 8, respectively. From the results, it can be seen that the exact pose of the parallel manipulator's moving platform can be precisely predicted using the identified kinematic parameters in the two steps. And the mean position and orientation errors of the validation configurations have been reduced to 1.56×10^{-4} m and 1.13×10^{-3} rad, respectively. As a comparison, the mean position and

https://doi.org/10.1017/S0263574718001352 Published online by Cambridge University Press

orientation errors according to the nominal kinematic parameters of the parallel manipulator are also calculated as 1.64×10^{-2} m and 6.46×10^{-2} rad, respectively. In other words, the positioning accuracy of the studied 3-PRS parallel manipulator has been significantly improved using the two-step calibration method proposed in this paper.

5. Conclusion

In this paper, a two-step parameter identification method is proposed for the kinematic calibration of the 3-PRS parallel manipulator. Using the proposed method, parameter identification of the studied parallel manipulator can be accomplished by means of two simple steps according to the limbs' geometric constraints. The spatial planes where the PRS limbs are locating are identified first as the geometric characteristics, which determine both the parasitic motions of moving platform and the locations of prismatic joints. The main advantage of the proposed calibration method is the simplification of error modeling. Only two simple geometric problems, rather than complex system error models, are required to identify the manipulator's kinematic parameters. Then, gradient-based searching algorithms can be used to solve the optimization problems efficiently. Calibration experiments are conducted on an apparatus of the studied parallel manipulator to validate the proposed method. From the results, it is seen that the kinematic parameters can be quickly identified by using the proposed two-step calibration method. And the positioning accuracy of the manipulator's moving platform can be significantly improved by means of the actual kinematics in terms of the identified parameters. Further, by a proper definition of geometric characteristics, the proposed two-step calibration method can also be extended to the kinematic parameter identification of other limited-DOF parallel manipulators.

Acknowledgments

This research was supported in part by the National Key Research and Development program of China under Grant No. 2017YFE0111300 and the Natural Science Foundation of China (NSFC) under Grants No. 51505279 and No. 51875334.

References

1. V. Nabat, M. Rodriguez, O. Company, S. Krut and F. Pierrot, "Par4: Very High Speed Parallel Robot for Pick-and-Place," *2005 IEEE/RSJ International Conference on Intelligent Robots and Systems*, Edmonton, Canada (2005) pp. 553–558.
2. X. Chu, F. Gao, W. Guo and C. Yan, "Complexity of heavy-payload forging manipulator based on input/output velocity relationship," *Proc. Inst. Mech. Eng. Part C: J. Mech. Eng. Sci.* **224**(11), 2468–2476 (2010).
3. G. Chen, H. Wang, K. Zhao and Z. Lin, "Modular calculation of the Jacobian matrix and its application to the performance analyses of a forging robot," *Adv. Rob.* **23**(10), 1261–1279 (2009).
4. L. Kong, G. Chen, H. Wang and Y. Zhao, "An Experimental Comparison for the Accuracy Improvement of a 6-PSS Parallel Manipulator by Choosing Different Sets of Measurement Data," *International Conference on Intelligent Robotics and Applications* (Springer, 2015) pp. 173–184.
5. T. Li, F. Li, Y. Jiang, J. Zhang and H. Wang, "Kinematic calibration of a 3-P(Pa)S parallel-type spindle head considering the thermal error," *Mechatronics* **43**, 86–98 (2017).
6. J. Wu, J. Wang, L. Wang and T. Li, "Dynamics and control of a planar 3-DOF parallel manipulator with actuation redundancy," *Mech. Mach. Theory* **44**(4), 835–849 (2009).
7. J. Wu, G. Yu, Y. Gao and L. Wang, "Mechatronics modeling and vibration analysis of a 2-DOF parallel manipulator in a 5-DOF hybrid machine tool," *Mech. Mach. Theory* **121**, 430–445 (2018).
8. J. Wu, J. Wang and Z. You, "An overview of dynamic parameter identification of robots," *Rob. Comput. Integr. Manuf.* **26**(5), 414–419 (2010).
9. W. Khalil and E. Dombre, *Modeling, Identification and Control of Robots* (Hermes Penton, London, UK, 2002).
10. Y. Liu, J. Wu, L. Wang, J. Wang, D. Wang and G. Yu, "Kinematic calibration of a 3-DOF parallel tool head," *Ind. Rob. Int. J.* **44**(2), 231–241 (2017).
11. H. Zhang, G. Cheng, X. Shan and F. Guo, "Kinematic accuracy research of 2(3HUS+S) parallel manipulator for simulation of hip joint motion," *Robotica* **36**(9), 1386–1401 (2018).
12. L. Kong, G. Chen, Z. Zhang and H. Wang, "Kinematic calibration and investigation of the influence of universal joint errors on accuracy improvement for a 3-DOF parallel manipulator," *Rob. Comput. Integr. Manuf.* **49**, 388–397 (2018).
13. G. Chen, L. Kong, Q. Li, H. Wang and Z. Lin, "Complete, minimal and continuous error models for the kinematic calibration of parallel manipulators based on poe formula," *Mech. Mach. Theory* **121**, 844–856 (2018).

14. A. Nubiola and I. Bonev, "Absolute calibration of an ABB IRB 1600 robot using a laser tracker," *Rob. Comput. Integr. Manuf.* **29**(1), 236–245 (2013).
15. G. Chen, H. Wang and Z. Lin, "Determination of the identifiable parameters in robot calibration based on the POE formula," *IEEE Trans. Rob.* **30**(5), 1066–1077 (2014).
16. W. Wang, H. Song, Z. Yan, L. Sun and Z. Du, "A universal index and an improved PSO algorithm for optimal pose selection in kinematic calibration of a novel surgical robot," *Rob. Comput. Integr. Manuf.* **50**, 90–101 (2018).
17. J. Wang and O. Masory, "On the Accuracy of a Stewart Platform. I. The Effect of Manufacturing Tolerances," *Proceedings of the 1993 IEEE International Conference on Robotics and Automation*, Atlanta, Georgia (1993) pp. 114–120.
18. O. Masory, J. Wang and H. Zhuang, "On the Accuracy of a Stewart Platform. II. Kinematic Calibration and Compensation," *1993 IEEE International Conference on Robotics and Automation, 1993, Proceedings*, Atlanta, Georgia (IEEE, 1993) pp. 725–731.
19. J. Hollerbach and D. Lokhorst, "Closed-loop kinematic calibration of the RSI 6-DOF hand controller," *IEEE Trans. Rob. Autom.* **11**(3), 352–359 (1995).
20. Y. Hu, F. Gao, X. Zhao, B. Wei, D. Zhao and Y. Zhao, "Kinematic calibration of a 6-DOF parallel manipulator based on identifiable parameters separation (IPS)," *Mech. Mach. Theory* **126**, 61–78 (2018).
21. J. Guo, D. Wang, R. Fan, W. Chen and G. Zhao, "Kinematic calibration and error compensation of a hexaglide parallel manipulator," *Proc. Inst. Mech. Eng. Part B: J. Eng. Manuf.* **233**(1), 215–225 (2019).
22. H. Zhuang, "Self-calibration of parallel mechanisms with a case study on stewart platforms," *IEEE Trans. Rob. Autom.* **13**(3), 387–397 (1997).
23. H. Zhuang, J. Yan and O. Masory, "Calibration of stewart platforms and other parallel manipulators minimizing inverse kinematic residuals," *J. Rob. Syst.* **15**(7), 395–405 (1998).
24. Y. Chiu and M. Perng, "Self-calibration of a general hexapod manipulator using cylinder constraints," *Int. J. Mach. Tools Manuf.* **43**(10), 1051–1066 (2003).
25. A. Rauf and J. Ryu, "Fully Autonomous Calibration of Parallel Manipulators by Imposing Position Constraint," *Proceedings of the 2001 IEEE International Conference on Robotics and Automation*, vol. 3, Seoul, South Korea (2001) pp. 2389–2394.
26. T. Huang, D. Chetwynd, D. Whitehouse and J. Wang, "A general and novel approach for parameter identification of 6-DOF parallel kinematic machines," *Mech. Mach. Theory* **40**(2), 219–239 (2005).
27. G. Chen, H. Wang and Z. Lin, "Optimal kinematic calibration of the 6-UPS parallel manipulator", **In**: *Intelligent Robotics and Applications. ICIRA 2013. Lecture Notes in Computer Science* (J. Lee, M. C. Lee, H. Liu, and J. H. Ryu, eds.), vol. 8102 (Springer, Berlin, Heidelberg).
28. M. Verner, F. Xi and C. Mechefske, "Optimal calibration of parallel kinematic machines," *J. Mech. Des.* **127**(1), 62–69 (2005).
29. H. Wang and K.-C. Fan, "Identification of strut and assembly errors of a 3-PRS serial–parallel machine tool," *Int. J. Mach. Tools Manuf.* **44**(11), 1171–1178 (2004).
30. L. Yu, Y. Yan, S. Ren and J. Zhao, "Vision-Based Method of Kinematic Calibration and Image Tracking of Position and Posture for 3-RPS Parallel Robot," *2017 IEEE International Conference on Mechatronics and Automation (ICMA)*, Takamatsu, Japan (2017) pp. 1757–1762.
31. A. Pashkevich, D. Chablat and P. Wenger, "Kinematic calibration of Orthoglide-type mechanisms from observation of parallel leg motions," *Mechatronics* **19**(4), 478–488 (2009).
32. G. Gojtan, G. Furtado and T. Hess-Coelho, "Error analysis of a 3-DOF parallel mechanism for milling applications," *J. Mech. Rob.* **5**(3), 034501 (2013).
33. P. Bai, J. Mei, T. Huang and D. G. Chetwynd, "Kinematic calibration of Delta robot using distance measurements," *Proc. Inst. Mech. Eng. Part C: J. Mech. Eng. Sci.* **230**(3), 414–424 (2016).
34. A. Joubair, M. Slamani and I. A. Bonev, "Kinematic calibration of a five-bar planar parallel robot using all working modes," *Rob. Comput. Integr. Manuf.* **29**(4), 15–25 (2013).
35. Y. Jiang, T. Li, L. Wang and F. Chen, "Kinematic error modeling and identification of the over-constrained parallel kinematic machine," *Rob. Comput. Integr. Manuf.* **49**, 105–119 (2018).
36. J. Zhang, Q. Chen, C. Wu and Q. Li, "Kinematic calibration of a 2-DOF translational parallel manipulator," *Adv Rob.* **28**(10), 707–714 (2014).